Egypt. J. Chem. Vol. **68**, No. 4, pp. 491 - 507 (2025)

Egyptian Journal of Chemistry

http://ejchem.journals.ekb.eg/

Synthesis, spectroscopic characterization of Ag(I), Sm(III) and U(VI) chelates with furfuran derivative, Catalytic activity, DFT and Biological study

Huda E.M. Amin[a], Omyma A.M. Ali[a], Samir M. EL-Medani[b], Doaa A. Nassar[a]*

[a]*Chemistry Department, Faculty of Women for Arts, Science and Education, Ain Shams University, Cairo, Egypt.*

[b]*Chemistry Department, Faculty of Science, El-Faiyum University, El-Faiyum, Egypt*

Abstract

Three new Schiff base complexes of silver (I), samarium (III), and uranium (VI) have been prepared by thermal reaction of the metal and the Schiff base" **L"** prepared by the condensation of furfuran and naphthalene-1,8-diamine. The ligand **L** and its complexes were specified by using spectroscopic methods IR, ^{1}H NMR, Uv-visible, mass spectroscopic (MS) in addition to elementary analysis, magnetic moment, conductivity and (TGA/DTA), SEM, X-rays (XRD), and PL (photoluminescence) examinations. The nitrogen of the azomethine group and the oxygen atom of the furan ring serve as coordination sites for the ligand, L, which acts as a neutral bidentate-type. The Ag(I) complex has been proposed to have a tetrahedral structure, whilst the uranium (VI) and samarium(III) complexes possess six coordinated octahedral geometries with formulae of $[AgL(H_2O)_2].NO_3.2H_2O$, $[SmL_3](ClO_4)_3.H_2O$ and $[UO_2L_2](ClO_4)_2$. Thermal analysis of the complexes indicated the presence of hydrated water molecules in both silver and samarium complexes, besides a coordinated water molecule in the silver complex and confirmed the absence of both hydrated and coordinated water molecules in uranium complex. The magnetic measurements of both Ag(I) and U(VI) complexes proved a diamagnetic property, while the Sm(III) complex was paramagnetic. The conductance measurements of complexes detect their electrolytic nature. The X-ray diffraction pattern of the ligand and its Ag(I) and U(IV) complexes exhibit sharp peaks indicating their crystalline nature, while the Sm(III) complex was found amorphous in nature. All the synthesized compounds except U(VI) complex can potentially serve as photoactive materials. Gaussian 09 software could be utilized to optimize the geometry of both ligand and silver(I) complex and then. Consequently, using the DFT technique the bond length, angles of bonds, HOMO-LUMO energy gap, and quantum chemical parameters could be computed. The Sm(III) compound was discovered to catalyze dye degradation in the presence of H_2O_2, with a noticeable shift in the color of the product of the reaction with time and temperature. Although the ligand may not be act as antitumor drug, the Ag(I) complex may be considered a modest anticancer agent. Binding studies between ligand and Ag(I), Sm(III) and U(VI) complexes with the S. aureus receptor have been studied by molecular docking.

Keywords: Ag(I), Sm(III) and U(VI) chelate; Catalytic activity; DFT; Biological study; Molecular docking.

1. Introduction

Schiff bases have a different implementation in several fields, e.g., biological activity [1-3], heterogeneous catalysis [4], oxygen carriers [5], oxidation of alkenes to alkanes [6] and photoluminescent properties [7]. The luminescent properties of lanthanide complexes depend on the electronic configuration of f-orbitals in each metal and ligands. Lanthanide complexes are used in a variety of applications, including conversion of solar energy [8], luminous substrates in biomedicine [9], superconductors [10], sensors [11], lasers [12,13]. Also, they were employed in the medical profession for diagnostics and therapy due to their luminescence and magnetic properties [14]. In certain situations, the bonding between the ligands and the Lanthanide sites through the "antenna effect" produces photoluminescence [15]. The Schiff base derived from 2-furaldehyde and phenylenediamine reacts with the lanthanides La(III), Sm(III), Gd(III), Er(III) to form the corresponding solid and stable complexes[16]. The analytical analysis proposed the general formula of the complexes $[Ln(L^{1-3})_2(NO_3)_2]NO_3.nH_2O$ where (Ln = La, Sm, Gd, Er) and n = ½, 1 or 2. The spectroscopic studies suggested the coordination of the metal ions with ligands through eight bonds. Interestingly, samarium complexes $[Sm(L^{1-3})_2(NO_3)_2]NO_3.H_2O$ showed specific fluorescence properties. The coordination chemistry of lanthanides represents special attention areas for its potential applications in biomedical field area such as catalysis, sensor magnetism, electronics and optics [17,18]. In addition, the lanthanide with Schiff bases complexes could be utilized as fluorescent indicators for cancer biomarkers [19]. Samarium(III) complexes have a wide range of uses, including optical. characteristics, catalysis, imaging, material doping [20] and have a low luminescence intensity when compared to other rare-earth-based ions [21]. Recently, nanomaterials have been used to enhance the luminescence properties of Sm3+ ions. For example, Sm^{3+}-doped nanocrystals have been found to exhibit significantly enhanced luminescence in comparison to bulk substances owing to their high surface area and efficient energy transfer processes [22]. Silver and its compounds have been known as poisonous to bacteria, viruses, fungi and algae. Recently, silver or silver compounds are used in medical field as anti-microbial agent and used as catalysis [23,24]. The biological activities of many silver(I) complexes have also been reported [25]. The uses of Ag(I) complexes can explain the role of the anti-microbial

*Corresponding author e-mail: names@mail.com.; (Name of corresponding author).
Receive Date: 17 April 2024, Revise Date: 12 July 2024, Accept Date: 22 August 2024
DOI: 10.21608/EJCHEM.2024.280559.9604

action involved in the interactions with DNA [26,27]. Several furan derivatives were extracted from plants, fruits, oils [28]. During thermal food processing of carbohydrates and ascorbic acid from sugar-amino acid interactions, furan derivatives were obtained. Due to the presence of the furan or tetrahydrofuran ring including the structure of furan derivatives, they have active biological properties that allow them to produce several pharmaceutical drugs. Compounds including the furan ring are biologically active. Comparing the biological activity of silver(I) complexes with pyrrole, AgPy2c, and furan-2-carboxylate, AgFu2c, against selected microorganisms and cell lines it is found that the AgFu2c complex was only effective [29,30]. The uranyl ion, UO_2^{2+}, is highly stable due to the strong bond between the uranium and oxygen atoms $[O=U^{VI}=O]^{2+}$. Uranyl(VI) complexes demonstrate a variety of appealing physicochemical features, including photoluminescence, photocatalysis, and photochemical reactivity [31,32]. Our interest in synthesizing and characterization of biologically active Schiff bases, especially furan derivatives and their transition metal complexes, has encouraged us to continue to achieve the our previously published ligand,8-((furan-2-ylmethylene)amino)naphthalene-1-amine, [33] with some selected transition metals; Ag(I), Sm(III) and U(VI). DFT has been used to calculate the HOMO-LUMO energy gap and the quantum chemical variables from optimizing structures. Binding studies between the ligand and Ag(I), Sm(III) and U(VI) complexes with the S. aureus receptor have been studied by molecular docking.

2. Experimental

2.1. Materials

Furfuran, naphthalene-1,8-diamine and all metal salts employed in this study ($AgNO_3$, Sm_2O_3 and $UO_2(ClO_4)_2$ were obtained from BDH Chemicals Ltd, England. All solvents were of high purity. They were utilized without being purified further.

2.2. Physical measurement

FTIR (KBr pellets) was obtained using a Perkins Elmer, spectrophotometer type 1430. ^{1}H NMR spectra were acquired using a Brucker 500 MHz analyzer in DMSO-d_6 as solvent with tetramethyl silane (TMS) as the internal reference. The elemental composition of the substances was performed using element analyzer by Perkin-Elmer. An Electrothermal 9200 was used to determine the melting degrees. The complexes' molar conductance was estimated utilizing a Jenway 4010 conductance instrument. On a JMS-AX 500 spectrometer, mass-spectral investigations for the compounds (70 eV, EI) were measured. On a Sherwood magnetism balance, the magnetic moment values were calculated using the Guoy method. The LS50B Jenway 6270 Fluorimeter was used to examine the compounds using 1 cm pathlength quartz cuvettes. The setting of the instrument's excitation slit and emission slit was 5 nm. Thermogravimetric measurements (TG and DTG) were performed utilizing a Shimadzu DT-50 thermal analyzer. PXRD imaging was done at room temperature using a Philips X'pert multifunctional diffraction and radiation sources{$K_{\alpha1}$(1.54056Å), $K_{\alpha2}$(1.54439Å) and K_β (1.39222 Å) with the intensity of radiation average weighted as ($K_\alpha$ave) 1.54184Å}.

2.3. Preparation of compounds

2.3.1 The synthesis of the ligand (L)

The synthesis of the ligand (L) was achieved by applying previously published procedures as described [33].

2.3.2 Synthesis of metal complexes

To prepare the complexes, 10ml, 1mmol of the metal salt solution was dissolved into absolute ethyl alcohol and the ligand was prepared by dissolving 1mmol of L in ethanol solution. The metal salt solution was added dropwise to the ligand solution with constant stirring. The resulting mixture was refluxed for three hours. Then, the resultant solution was concentrated by evaporation. The formed precipitate was isolated and washed several times by hot petroleum ether. The proposed structure of complexes is given in Fig. 1.

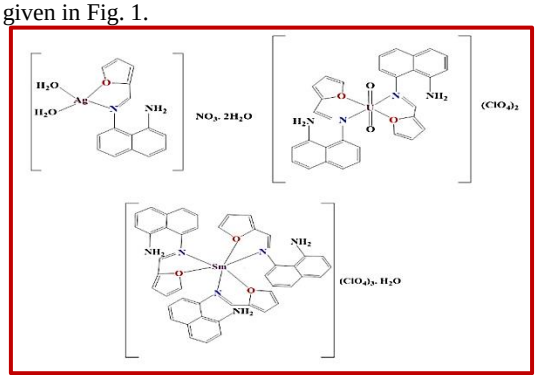

Fig. 1: The proposed structure of complexes.

2.4. DFT computations

Using the DFT approach, the ligand and Ag(I) complex structure were optimized in the gas phase. Gaussian 09 software was used for all calculations. The B3LYP functional used the 6-31G(d) ligand basis set and the LanL2DZ complex basis set. The orbital energy was calculated using the optimized structures.

2.5. Catalytic activity of Sm(III) complex

The experiment was carried out in a thermostatic water bath with constant concentrations of the methyl orange dye (MO) solution (0.015 gm/L), hydrogen peroxide (1.0 mL), and Sm(III) complex catalyst (0.003gm) at three distinct temperatures of 40, 50, and 60 ^{o}C. A magnetic stirrer was used to stir the reaction mixture. The wavelength of absorption of the combination was evaluated at 470 nm at various times and temperatures using extracted parts of the thermostatic reacting mixture.

2.6. Pharmacological evaluation

2.6.1. Antimicrobial activity in vitro

The fungus *A. flavus and C. albicans*, the bacteria *S. aureus, E. coli, B. subtilis*, and *P. aeruginosa*, as well as the standards Ampicillin and Amphotricine B, were utilized in this investigation. Activities of all synthesized compounds were examined employing NA (Nutrient Agar) and Sabouraud dextrose-agar (SDA) media growing bacteria and fungus [34,35]. The examined compounds were dissolved into a small quantity of DMSO to attain concentrations equal to 1 mg/ml, and 100 µl for every preparation utilized. The plates made of agar were left to incubate at 37°C for bacteria and 25°C for fungi, respectively. The widths of inhibitory growth areas in millimeters during 24 hours to supply bacteria and 48 hours to supply fungi were measured as an indication of antimicrobial activity. The test was performed in duplicate. The zone dimension measurements were averaged and the average values were recorded. The outcomes were classified as either inactive, little activity, medium activity, or significant activity.

2.6.2. Minimum Inhibitory Concentration (MIC) Determination

The MIC is defined as the smallest concentration of an antimicrobial substance or investigated substance which will suppress detectable growth of bacteria during overnight incubation in comparison to the control substance. Bacterial stationary-phase cultures were produced at 37°C and utilized to infuse in new 5.0 ml of the culture to achieve an OD600 of 0.05. After incubation the 5.0 ml cells at 37 °C for OD600 of 0.10, calibrated suspensions of bacteria were produced to the last density of cells of 6 x 10^5 CFU/ml. Before applying the extracts to the plates and incubating them for 24 hours at 37°C, multiple dilutions (0-128g/ml) were made and mixed with 5.0 ml of the optimized bacteria solution. Colony formation units (CFU) were measured for each concentration (NCCLS: M7-A4, 1997) [36].

2.7. Cytotoxicity evaluation using viability assay

Human breast cancer (MCF-7) cells were used in an in vitro screening test for the ligand and Ag(I) complex at the Regional Centre for Mycology and Biotechnology, Cancer Biology Department, Pharmacology Department, Al Azhar University using cisplatin standard. The cells were obtained from the American Type Culture Collection (ATCC, Rockville, MD). The cells were cultured in 10% heat inactivated fetal bovine serum (FBS), 50 g/ml gentamycin, 1% L-glutamine, 10% Dulbecco's altered Eagle's medium (DMEM), and a buffering agent called HEPES. Every cell was cultured two times for a week in a humid environment using 5% CO_2 at 37ºC. For the cell toxicity experiment, the embryonic stem cells are placed in a plate with 96 holes. New medium with varying amounts of the analyzed samples being injected after 24 hours. A variety of channel pipes were employed to deliver sequential double-dilutions of the examined substance to single merged cell layers. For 48 hours, a humidified chamber with 5% CO_2 and 37°C was used to incubate microtiter dishes. For every sample dosage, three separate wells were employed. The tiny amount of DMSO found in the holes (up to 0.1%) had no influence on the experiment. After 24 hours of growth at 37°C, different quantities of samples were administered, and the surviving cell generated was investigated. Following the completion of the incubation phase, fresh media was extracted and a 1% crystalline violet fluid was introduced to every well for a minimum of 30 minutes. The spot was eliminated and the serving dishes were thoroughly cleaned with water from the tap to eliminate any leftover stains. The absorbance was measured at 490. All data has been modified using baseline absorbance determined in wells with no additional staining. The treatment specimens were contrasted with the cellular control in having no of the investigated chemicals. Every procedure was done in triplicate. For each tested compound's cell, cytotoxicity was calculated. To determine the quantity of active cells, a reader for micro plates was used for figuring out the density of optics. By charting the association between remaining cells and medication concentration, the remainder curve of every cell was established.

Table 1: Physical and analytical data of the metal complexes

Compound	Color	M.P	Yield (%)	C% Obs. (Cald.)	H% Obs. (Cald.)	N% Obs. (Cald.)	Molar conductance ($\Omega^{-1}mol^{-1}$ cm^2)
$[AgL(H_2O)_2]NO_3.2H_2O$ $AgC_{15}H_{20}N_3O_8$	Brown	>300	75	37.4 (37.7)	3.9 (4.2)	8.2 (8.8)	55
$[SmL_3](ClO_4)_3.H_2O$ $SmC_{45}H_{38}N_6O_{16}Cl_3$	Dark brown	>300	85	46.4 (46.0)	3.1 (3.3)	6.8 (7.1)	330
$[UO_2L_2](ClO_4)_2$ $UC_{30}H_{24}N_4O_{12}Cl_2$	Black	>300	83	38.7 (38.2)	2.8 (2.5)	6.1 (5.9)	202

Table 2: FTIR and 1H NMR spectral information about the ligand and its metal complexes (cm-1)

Compounds	ν(NH_2) Or (OH)	ν(C=N)	ν(C-O-C) (furan)	ν(M-O)	ν(M-N)	Additional bands	^{1}H NMR (ppm)
L	3345, 3309	1632	1243	-	-	-	10.68 s (2H, NH_2), 7.92 (1H, azomethine), 6.23-7. m (9H (6ArH, 3 Furan H))
$[AgL(H_2O)_2]NO_3.2H_2O$	3395	1635	1270	524	480	1383, 821 νNO_3 ionic	10.68 s (2H, NH_2), 8.34 s (1H, azomethine), 6.81-7.90 m (9H (6ArH,
$[SmL_3](ClO_4)_3.H_2O$	3420	1645	1270	525	473	1117, 627 ν(ClO_4^-)	-
$[UO_2L_2](ClO_4)_2$	3345	1644	1270	524	470	1119, 625 ν(ClO_4^-) 1088 ν(O=U=O)	10.68 s (2H, NH_2), 8.30 s (1H, azomethine), 6.20-7.90 m (9H (6ArH, 3Furan H))

The fifty percent concentration that inhibits (IC50), or the amount of substance needed to elicit adverse effects in fifty per cent of cells that are not damaged, was determined using the graphing tool utilizing graphic graphs of the dosage responsiveness curve for every concentration [37,38].

3. Results and discussion

3.1. Elemental examinations

Table 1 showd the outcomes of the analysis (CHN) data including proposed chemical formulas and physical parameters of complexes of Schiff base. The Ag(I), Sm(III, and U(VI) complexes were insoluble in the majority of popular solvents containing organic compounds except DMF and DMSO.

3.2. Magnetic and electrical conductivity investigations

Magnetic moment studies demonstrated that the two Ag(I) and U(VI) complexes have a diamagnetic property [39], while that of the Sm(III) complex has a paramagnetic property with a value of 1.56 BM. [40].The conductivity measurements of all complexes examined in DMF demonstrated the electrolyte character (Table 1). According to the observed values, the compounds seemed electrolytes in order of kind 1:1 just for the Ag(I) complex, 1:2 for the U(VI) complex, and 1:3 for the Sm(III) complex.

3.3. IR and ^{1}H NMR spectra

The infrared spectroscopy for compounds indicated substantial ν(C=N) within a 1635-1645 cm^{-1} region, with some shift compared to that of the ligand (1632 cm^{-1}) [41-43]. Furthermore, IR spectra revealed ν(NH_2) and/or ν(H_2O) broad stretching frequencies within the 3345-3420 cm^{-1} range (Table 2). These observations could imply that the complexes included coordination or hydrated water molecules. Moreover, the band at 1270 cm^{-1} in the spectra of complexes may be due to ν(C-O-C) [44]. Non-ligand vibrations that stretching were also identified in the infrared spectra of complexes at the 525-524 cm^{-1} and 480-470 cm^{-1} areas were dubbed ν(M-O) and ν(M-N) stretched vibration, consequently, and confirmed binding of the atoms of oxygen and nitrogen to the metal in complexes [45]. Furthermore, the FTIR spectrum of the Ag(I) complex showed bands at 1383 and 821 cm^{-1} that matched with the ionic nitrate group [46]. Other bands appeared at 1117 and 627 cm^{-1} in the IR spectroscopy of the Sm(III) complex owing to ν(ClO_4^-) stretched frequency, while the U(VI) complex showed stretching bands of frequencies at 1119 and 625 cm^{-1}due to the inclusion of ClO_4^- ion, in U(VI) complex, in addition to stretching band of frequency at 1088 cm^{-1}corresponding to O=U=O species [47].The one-dimensional nuclear magnetic resonance values of the ligand L, as well as the Ag(I) and U(VI) complexes were recorded. For the ligand L, the ^{1}H NMR spectrum demonstrates an NH_2 singlet at 10.68 ppm [48] while the two Ag(I) and U(VI) complexes exhibited no shift in NH_2 protons compared to the ligand. In addition, the ^{1}H NMR spectra for the two complexes (Figure 2) revealed singlets at 8.35 and 8.30 ppm owing to the azomethine group for Ag(I) and U(VI) complexes, respectively, with a lower field shift than the corresponding signal in ligand (7.92 ppm). These findings verified metal-ligand coordination via the O of the furan molecule as well as the N of the azomethine. Furthermore, the aromatic and furan protons of the ligand (6.23-7.52 ppm) exhibited proper shift in complexation (6.20-7.90 ppm) (Table 2).

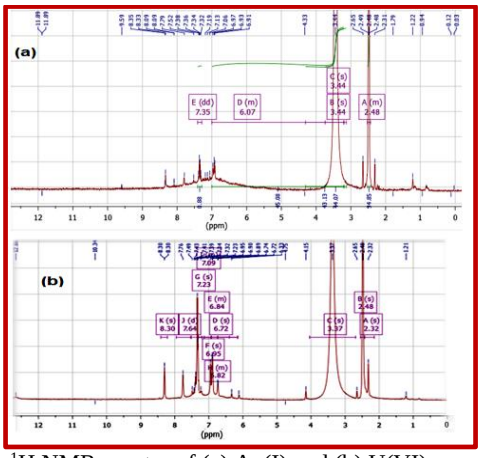

Fig. 2: ^{1}H NMR spectra of (a) Ag(I) and (b) U(VI) complexes.

3.4. Mass spectra

Mass spectrometry measurements of Ag(I) as well as U(VI) compounds (Figure 3) revealed peaks for molecular ions at m/z = 479 (42%) and m/z = 942 (29%) which agree with the suggested molecular weight 478.206 and 941.475 amu, respectively.

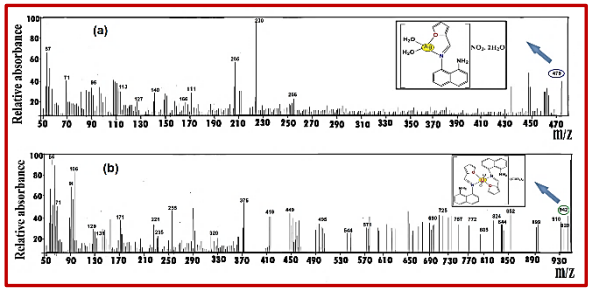

Fig. 3 : Mass spectra of (a) Ag(I) and (b) U(VI) complexes.

3.5. Electronic spectra

At ambient temperature, electronic characteristics for the compounds were obtained (Figure (4a, b) & Table 3). The complexes' absorption spectra showed two distinct bands at 274–281 nm and 328–345 nm, as well as a novel band around (429–447 nm) that was associated with π→π*, n→π* and charge transfer (C.T) transitions, respectively [49].

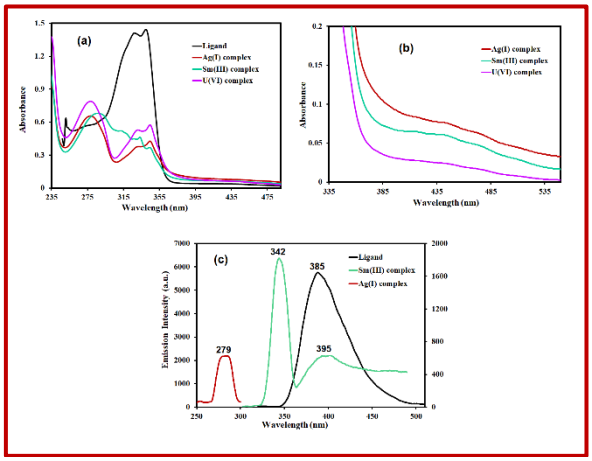

Fig. 4: The UV-Vis (a, b) and fluorescence spectra (c) of synthesized ligand and its metal complexes.

Table 3: Electronic spectra data λ (nm) of the ligand, L and its metal complexes.

Compound	UV-Vis data λ_{max}		
	$\pi\rightarrow\pi^*$	$n\rightarrow\pi^*$	CT
L	252	329,340	-
$[AgL(H_2O)_2]NO_3.2H_2O$	274	345	447
$[SmL_3](ClO_4)_3.H_2O$	281	332	438
$[UO_2L_2](ClO_4)_2$	274	328,344	429

3.6. Photoluminescence studies

The spectra of fluorescence for the L and Ag(I) and Sm(III) compounds (Figure 4c) in DMF solution were determined at room temperature. Some ligands of Schiff bases with an aromatic ring can have their fluorescence emission improved or inhibited by metal ions. Transition metal ion quenching of ligand fluorescence upon complexation was a fairly typical phenomenon which was attributed to mechanisms such as magnetic disturbance and electrical energy transfer [50]. The ligand's fluorescence was quenched via an Ag(I) ion, which exhibited a maximum of 279 nm on excitation at 274 nm. However, the emission intensity for the Sm(III) complex was stronger compared to that of the ligand, found at 342 nm and 395 nm when stimulated at 281 nm, respectively. The U(VI) complex exhibited no emission when excited at 344 nm. On the other hand, fluorescence enhancement via complexation piqued our attention because it opens the door to photochemical applications for these complexes [51].

3.7. Thermal and kinetic studies

The thermogravimetry plot revealed that the $[AgL(H_2O)_2]NO_3.2H_2O$ complex breaks down into three distinct stages (Figure5). The first breakdown peak took place between 44-160 ^oC degrees Celsius, along with a loss of mass of 14.78% (calc. 15.06%), representing the loss of $4H_2O$. The next breakdown stage (160-299 ^oC, 10.70 %) caused the removal of $NO_2+½O_2$ species. Whereas, the third breakdown phase, occurred at temperatures ranging from 299 to 415 ^oC and results in a loss of weight of 51.50% due to the removal of the $C_{15}H_{12}N_2O$ moiety, releasing metallic silver as residue (Table 4).

The $[SmL_3](ClO_4)_3.H_2O$ TG plot revealed three breakdown stages in the average temperature of 28-1000 ^oC (Figure 5). The initial stage of breakdown proceeded at temperatures ranging from 28 to 110 ^oC and produced an overall loss of weight 9.96 % owing to the loss of H_2O and $2NO_2$ molecules. A 2nd breakdown step with a mass loss of 29.21% took place within the temperature range 110-325 ^oC, related to the decomposition of the $[C_{15}H_{12}N_2O+3HCl]$ species. The last breakdown stage occurred at temperatures ranging from 325-1000 degrees Celsius and resulted in a loss of weight of 46.44% owing to the removal of $C_{30}H_{21}N_2O_7+ ½O_3$ moieties, leaving metallic $½Sm_2O_3$ as a residue (Table 4).

Table 4: Thermogravimetric data of the metal complexes

Compound	Stage	Temp. range (°C)	Mass loss (%)		Evolved moiety	Residue (%) Found (Calc.)
			Found	Calc.		
$[AgL(H_2O)_2]NO_3.2H_2O$	I	44-160	14.78	15.06	$2H_2O$(hyd.)+$2H_2O$(coord.)	Ag 23.02 (22.57)
	II	160-299	10.7	11.29	$NO_2+½O_2$	
	III	299-415	51.5	51.08	$C_{15}H_{12}N_2O$	
$[SmL_3](ClO_4)_3.H_2O$	I	28-110	9.96	9.36	H_2O(hydrated), $2NO_2$	$½Sm_2O_3$ 14.83 (14.39)
	II	110-325	29.21	29.40	$C_{15}H_{12}N_2O+3HCl$	
	III	325-1000	46.44	46.41	$C_{30}H_{21}N_2O_7+ ½O_3$	
$[UO_2L_2](ClO_4)_2$	I	30-85	3.47	3.00	C_2H_4	UO_3 29.60 (30.06)
	II	85-298	26.85	27.62	$2HCl+C_{15}H_7$	
	III	298-906	40.40	40.00	$C_{13}H_{11}N_4O_9$	

The thermal decomposition plot of $[UO_2L_2](ClO_4)_2$, showed thermal decomposition in three stages ranging from 30 to 906 ^oC (Figure5). The initial breakdown stage appeared in temperatures ranging from 30 to 85^oC, with a total weight loss of 3.47% (3.00%), which might have contributed to C_2H_4 moiety. The second step took place at 85-298 ^oC and caused a total mass loss of 26.85% (27.62%), probably due to the removal of $2HCl+C_{15}H_7$. The final breakdown stage, which occurs at temperatures ranging from 298-906 degrees Celsius and results in a total loss of weight of 40.40% (40.00%), may correlate to the elimination of $C_{13}H_{11}N_4O_9$, remaining a residue of UO_3 of 29.60% (30.06%) (Table 4).

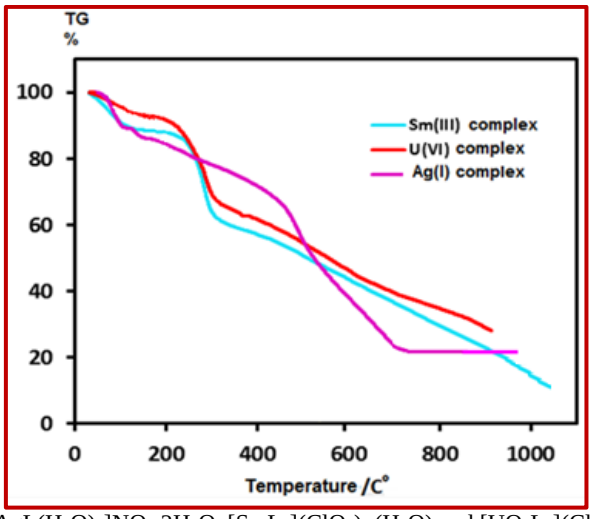

Fig. 5: TG of $[AgL(H_2O)_2]NO_3.2H_2O$, $[SmL_3](ClO_4)_3(H_2O)$ and $[UO_2L_2](ClO_4)_2$ complexes.

Thermodynamic parameters of the complexes process of decomposition were calculated [52]. Table 5 shows the computed and tabulated parameters of kinetics including (S*) activation entropy, (G*) activation energy and (H*) activation enthalpy. The energy of activation of decomposition, E*, was observed to be in the 34-156 kJ mol^{-1} range, indicating that the complexes are thermally stable.

This pattern of performance is acceptable with the covalent nature of the compounds [53,54]. Negative S* values, on the other hand, imply a more organized activated complex with a lower rate of decomposition processes than normal [55,56].

3.8. Optical properties for the prepared complexes

The energy of the band gap (E_{opt}) was calculated using ultraviolet -visible absorption spectra. The value of optical band gap energy (E_{opt}) was calculated using the Tauc relation, which is the relationship between the coefficients of absorption α and the energy of the photon hν for indirect transition as $(\alpha h\nu)^{1/2} = A(h\nu - E_{opt})$, where A is a constant [57]. According to Figure 6 (a-c), the calculated values of E_{opt} for Ag(I), Sm(III), and U(VI) complexes were 3.14, 3.10, and 3.20 ev, respectively. As a result, we may expect that the complexes may be employed as semiconductors in solar cell applications [58].

3.9. Powder XRD analysis

Because many efforts to generate a single of complexes failed, the crystalline structure of these complexes was established via diffraction of X-ray powder research. The patterns of X-ray diffraction of all recently produced molecules have been scanned across the 2θ=10°-80° range at a wavelength of 1.540

Å. The Sm(III) complex (Figure7) was discovered to be an amorphous (non-crystalline).The ligand and its Ag(I) and U(VI) compounds had strong peaks in their diffraction by X-ray patterns, confirming their

Table 5: Thermodynamic parameters of the thermal decomposition of the metal complexes

Compound	Steps	Decomposition Temp. range ˚C	DTGA peak ˚C	A (s^{-1})	ΔH^* (KJ/mol)	ΔS^* (J/mol)	ΔG^* (KJ/mol)	E* (KJ/mol)	R^2
$[AgL(H_2O)_2]NO_3.2H_2O$	I	88-153	131	23.82	36.90	-163.68	103.09	40.26	0.9610
	II	165-201	180	6.28	35.01	-175.71	114.62	38.78	0.9420
	III	383-400	395	18.60×10^7	150.71	-36.12	175.51	156.42	0.9830
$[SmL_3](ClO_4)_3.H_2O$	I	28-128	64	97.06×10^3	39.25	-136.72	48.06	39.79	0.9817
	II	229-328	278	12.55×10^4	60.26	-147.76	10.15	62.93	0.9801
$[UO_2L_2](ClO_4)_2$	I	29-148	67	8.3×10^3	33.65	-157.45	44.24	34.21	0.9846
	II	203-322	283	5.55×10^3	47.07	-172.84	96.08	49.43	0.9627

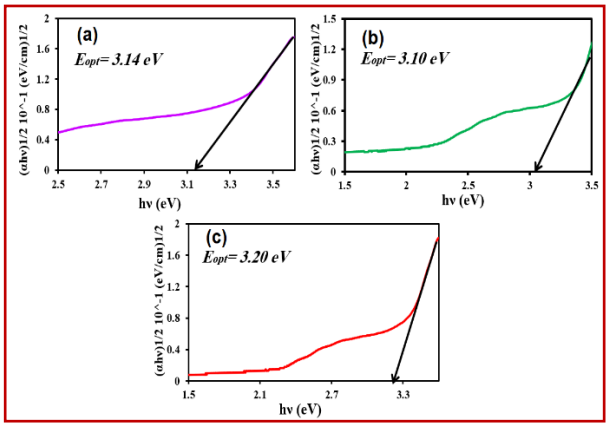

Fig. 6: Optical band gap for (a) $[AgL(H_2O)_2]NO_3.2H_2O$, (b) $[SmL_3](ClO_4)_3(H_2O)$ and (c) $[UO_2L_2](ClO_4)_2$

crystallized nature. Table 6 lists the XRD data acquired, such as (I) the relative intensities, d-spacing and 2θ. The reported and calculated values of d-spacing were contrasted. When the total diffractograms of metal complexes with and without the free ligand, L, were contrasted, it was obvious that the disappearance of ligand peaks and the emergence of novel peaks indicated the production of metal complexes [59]. The particle size was estimated using the Debye-Scherrer equation [60]. The average particle sizes of the ligand, Ag(I), and U(VI) complexes were 18.69, 11.66, and 7.06 nm, respectively, indicating that they were nanocrystalline.

The relationship $\delta = 1/D^2$ (where δ is the dislocation density in nm^{-2}) was used to calculate the dislocation density, which was the number of dislocation lines per unit area of the crystal (Table 7) [61].

Table 6: X-ray diffraction data of the ligand and U(VI) and Ag(I) complexes

Peak no.	Ligand				$[UO_2L_2](ClO_4)_2$				$[AgL(H_2O)_2]NO_3.2H_2O$			
	d(Å)		Intensity (%)	Angle (2*Θ*)	*d*(Å)		Intensity (%)	Angle (2*Θ*)	*d* (Å)		Intensity (%)	Angle (2*Θ*)
	Obs.	*Calc.*			*Obs.*	*Calc.*			*Obs.*	*Calc.*		
1	4.86	4.86	95.11	18.21	7.78	7.78	5.23	11.36	2.49	2.5	1.80	35.91
2	4.96	4.96	78.28	17.86	4.80	4.80	4.08	18.43	2.40	2.40	10.20	37.37
3	3.97	3.97	62.90	22.35	3.69	3.69	8.48	24.03	2.36	2.36	100.00	38.04
4	3.60	3.60	53.11	24.68	3.12	3.12	100.00	28.50	2.04	2.04	20.09	44.24
5	6.77	6.77	45.55	13.04	2.70	2.70	35.83	33.03	1.66	1.66	0.53	55.20
6	5.97	5.97	25.43	14.80	1.91	1.91	36	47.37	1.44	1.45	29.32	64.44
7	4.65	4.65	23.66	19.04	1.63	1.63	31.15	56.24	1.33	1.33	1.40	70.72
8	4.62	4.62	21.51	19.17	1.56	1.56	4.92	58.90	1.23	1.23	30.03	77.37
9	3.77	3.77	100.00	23.51	1.35	1.35	3.18	69.19	-	-	-	-
10	4.37	4.37	22.84	20.25	7.78	7.78	5.23	11.36	2.49	2.5	1.80	35.91

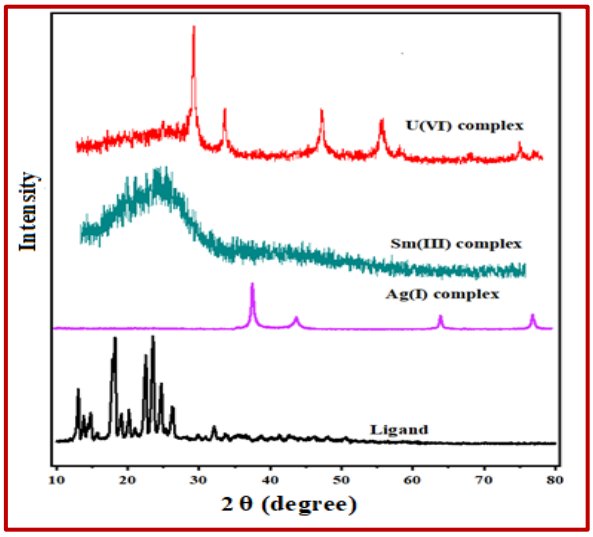

Fig. 7: X-ray diffraction patterns of the ligand and its complexes.

Table 7: Geometric parameters data of the prepared ligand and Ag(I) and U(VI) complexes.

Compound	Geometric parameters data				
	Angle (2Θ)	d (Å)	FWHM (radian)	D (nm)	δ (nm^{-2})
L	23.51	3.78	9.5×10^{-3}	18.69	8.2×10^{-4}
$[AgL(H_2O)_2]NO_3.2H_2O$	38.05	2.36	9.53×10^{-3}	11.66	1.10×10^{-4}
$[UO_2L_2](ClO_4)_2$	28.50	3.13	2.08×10^{-2}	7.069	2×10^{-2}

3.10. Scanning electron microscopy (SEM)

Sm(III) and UO_2^{2+} complexes were examined using SEM at various magnifications (Figure 8). The Sm(III) complex particles indicated layers form while the UO_2^{2+} complex particles were found to have a surface morphology that is similar to needle-shaped objects with rough surfaces.

Table 8: Some selected bond lengths (Å) and bond angles (degrees) of the optimized geometry of ligand and its Ag(I) complex by using DFT/B3LYP levels of theory.

Bond length (Å)	Ag complex	Bond angle (°)	Ligand	Bond angle (°)	Ag complex
C21-N20	1.3740	N1-C21-C23	122.79	N20-C21-C22	126.958
Ag30-N20	2.2670	C21-C23-O25	119.45	C21-C22-O27	122.18
Ag30-O27	3.1980	N1C21C23O25	-0.841	N20-Ag30-O27	64.12
Ag30-O31	2.3730			N20-Ag30-O33	122.311
Ag30-O33	2.3540			O33-Ag30-O31	122.83
				N20C21C22O27	7.503

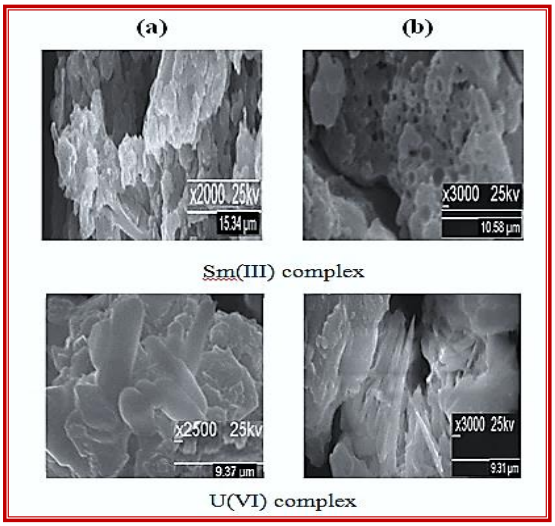

Fig. 8: SEM of Sm(III) and U(VI) complexes at low (a) and (b) high magnification.

3.11. Geometry optimization

During the absence of a single crystal X-ray data, the parameters of geometry of both the Schiff base and the Ag(I) complex was optimized using DFT to interpret its structural geometries. Figure 9 showed the optimum geometries and atoms with a number scheme of L and its Ag(I) complex. The bond lengths plus angles of bonds are shown in Table 8.

As binding occurs through N of the azomethine group, the length of the azomethine C21-N1 bond (1.2850Å) in the ligand grows somewhat longer in Ag(I) complex [62]. The average angles of bonds N20Ag30O33 and O33Ag30O31 within the Ag(I) complex were discovered to be within the 126.9° range around the atoms of metal, which differ significantly from those predicted for the square planar, suggesting a deformed tetrahedral structure [63].

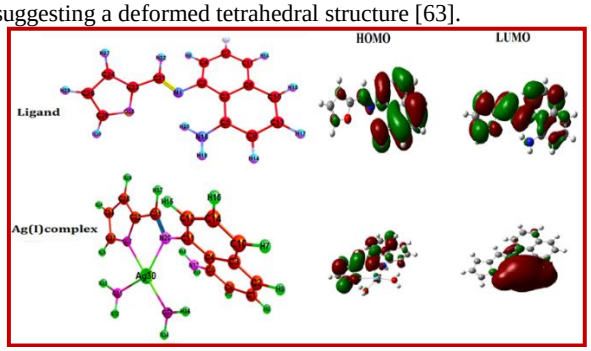

Fig. 9: The optimized structure and frontier molecular orbitals of the ligand and Ag(I) complex.

3.12. Frontier molecular orbital analysis

The HOMO-LUMO gap was calculated using density functional theory (DFT). The lower HOMO energy value indicated that the molecule's ability to donate electrons was limited. Conversely, a higher HOMO energy suggested that the molecular structure is an effective electron donor. The ability of a molecule to receive electrons is represented by LUMO energy. The HOMO-LUMO energy gap governs a molecule's stability and reactivity. Figure 9 gives the HOMO and LUMO orbital graphs corresponding to the L and Ag(I) complex evaluated in the gas phase. The shift in the centers in HOMO and LUMO inside the Ag(I) complex showed an electron density transfer within the complex. LUMO of the ligand was distributed throughout the ligand except for the amino group, whereas HOMO electron density was not found on furan oxygen. In the case of the silver complex, the HOMO was located on the whole compound while the LUMO location on the naphthalene ring has been decreased. The energy gap between HOMO and LUMO in the ligand was less than that of the Ag(I) complex [64]. The estimated parameters of quantum chemicals were shown in Table 9 as IP (the ionization potential), EA (electron affinity), χ (absolute electronegativities), σ (absolute softness), η(absolute hardness), S (global softness), μ (chemical potentials), ω (global electrophilicity) and ΔN_{max} (the additional electronic charge) [65].

3.13. Molecular docking studies

The MOA2019 programme was used to run molecular docking simulations in order to identify the binding of L and silver complex with the most active region of the gram-positive bacterium (*S. aureus*) receptor. According to the current work, the L, AgL, UO_2L_2 and SmL_3 with the protein receptor (PDB ID: 1jij) have binding free energies of -1.1, -140.4, -24.0 and -4.9 kcal/mol with the protein receptor (PDB ID: 1jij), respectively (Table 10 and Figure10). Stronger interactions result from more negative binding energies. Therefore, the interactions follow the pattern AgL>UO_2L_2 >SmL_3 > L.

Table 9: The calculated quantum chemical parameters for L and its Ag(I) complex.

Compound	E_{HOMO} (eV)	E_{LOMO} (eV)	ΔE (eV)	IP (eV)	EA (eV)	χ (eV)	η (eV)	σ $(eV)^{-1}$	μ (eV)	S $(eV)^{-1}$	ω (eV)	ΔN_{max}
L	-4.591	-1.79	2.80	4.59	1.79	3.19	1.40	0.71	-3.19	0.35	3.63	2.27
$[AgL(H_2O)_2]NO_3.2H_2O$	-4.207	-1.33	2.87	4.20	1.33	2.77	1.43	0.69	2.77	0.34	2.67	1.92

3.14. Catalytic activity of Sm(III) complex

3.14.1. The influence of time and temperature

Organic dyes are widely employed in a wide range of industries. This has caused a significant environmental issue with water pollution. In recent years, improved oxidation techniques, particularly in order to treat dye wastewater (e.g., H2O2, OH• radical), have received more attention to properly attack and degrade those organic contaminants [66]. The adsorption of methyl orange dye on the catalyst surface Sm(III) complex was performed in the presence of H2O2. It has been discovered that unless the catalyst and the oxidant are both present in the dye solution, no decolorization occurs. The percentage of methyl orange aqueous solution degradation over time at 40, 50, and 60°C was shown in Figure 11. It was obvious that the Sm(III) complex catalyzes dye decolorization with a significant shift in the color of the reaction mixture. Furthermore, as shown in Table 11, the absorption peak of the unreacted dye (A°/A) decreased with time at each temperature.

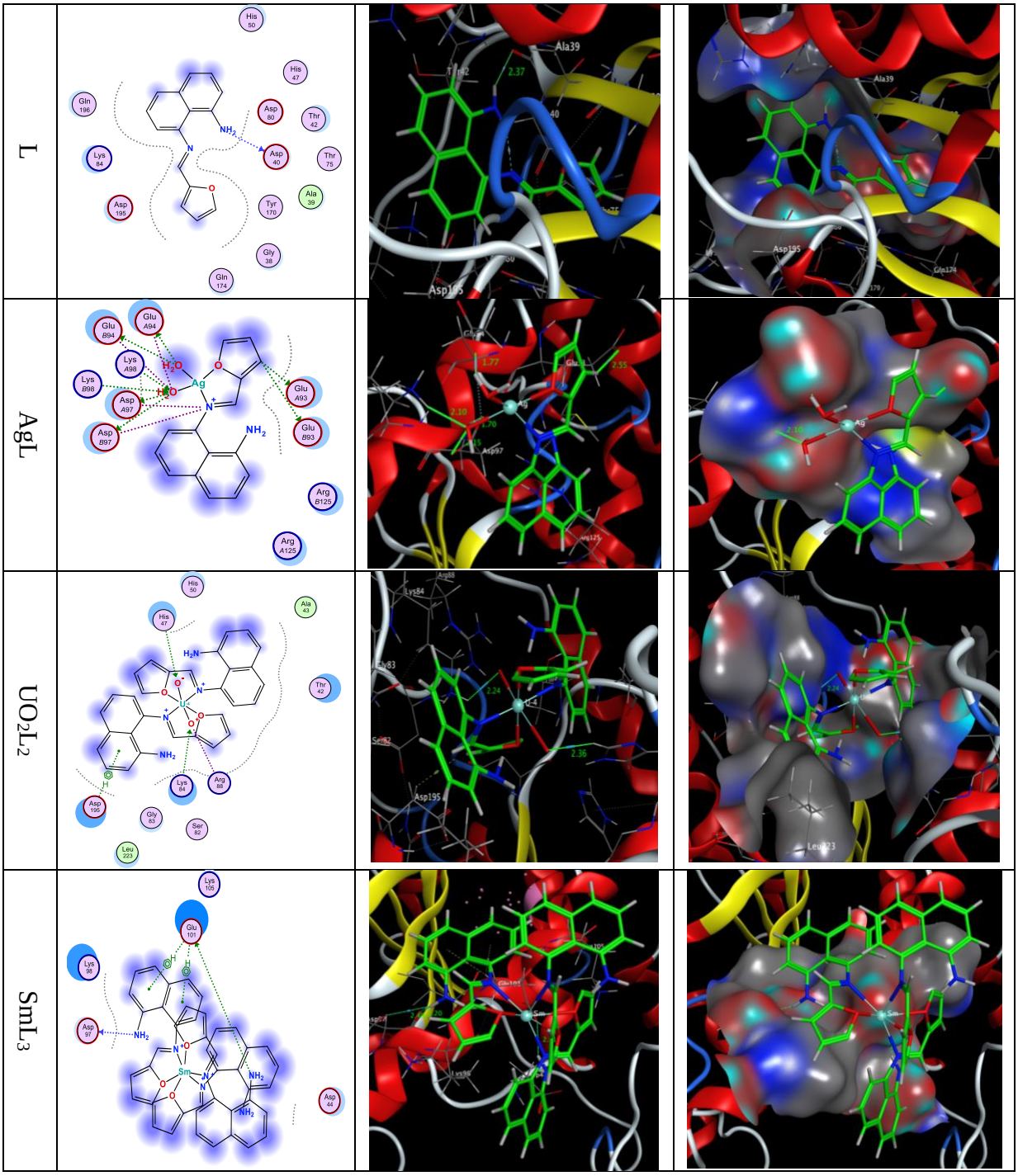

Fig. 10: 2D and 3D plots of the interaction between L, AgL, UO2L2 and SmL3 with the active site of the receptor of Staphylococcus aureus (PDB ID: 1jij). Hydrophobic interactions with amino acid residues are shown with dotted curves.

Table 10: The Docking interaction data of L, AgL, UO_2L_2 and SmL_3 with the active sites of the receptor S. aureus.

	Receptor	Interaction	Distance(Å)	E (kcal/mol)
L				
N 18	O ASP 40	H-donor	3.33	-1.1
AgL				-140.4
C 24	OE1 GLU 93	H-donor	3.52	-1.3
C 24	OE1 GLU 93	H-donor	3.52	-1.3
O 31	OE2 GLU 94	H-donor	2.63	-21.2
O 31	OE2 GLU 94	H-donor	2.63	-21.2
O 34	OD1 ASP 97	H-donor	2.74	-23.0
O 34	OD2 ASP 97	H-donor	2.77	0.8
O 34	OD1 ASP 97	H-donor	2.74	-23.0
O 34	OD2 ASP 97	H-donor	2.77	-0.8
O 34	NZ LYS 98	H-acceptor	3.08	-0.5
O 34	NZ LYS 98	H-acceptor	3.08	-0.5
N 1	OD1 ASP 97	Ionic	3.69	-1.2
N 1	OD1 ASP 97	Ionic	3.69	-1.2
O 31	OE2 GLU 94	Ionic	2.63	-7.5
O 31	OE2 GLU 94	Ionic	2.63	-7.5
O 34	OE2 GLU 94	Ionic	3.30	-2.8
O 34	OD1 ASP 97	Ionic	2.74	-6.5
O 34	OD2 ASP 97	Ionic	2.77	-6.2
O 34	OE2 GLU 94	Ionic	3.30	-2.8
O 34	OD1 ASP 97	Ionic	2.74	-6.5
O 34	OD2 ASP 97	Ionic	2.77	-6.2
UO_2L_2				-24.0
O 60	NZ LYS 84	H-acceptor	2.91 (2.24)	-10.3
O 61	CE1 HIS 47	H-acceptor	3.29 (2.36)	-2.8
O 60	NZ LYS 84	Ionic	2.91	-5.1
O 60	NH1 ARG 88	Ionic	2.90	-5.2
6-ring	CB ASP 195	pi-H	3.57	-0.6
SmL_3				-4.9
N 13	OE1 GLU 101	H-donor	2.89 (2.11)	-2.0
N 41	O ASP 97	H-donor	3.05 (2.20)	-0.8
N 41	OD2 ASP 97	H-donor	3.38 (2.49)	-0.8
6-ring	CB GLU 101	pi-H	4.23	-0.7
6-ring	CB GLU 101	pi-H	3.95	-0.6

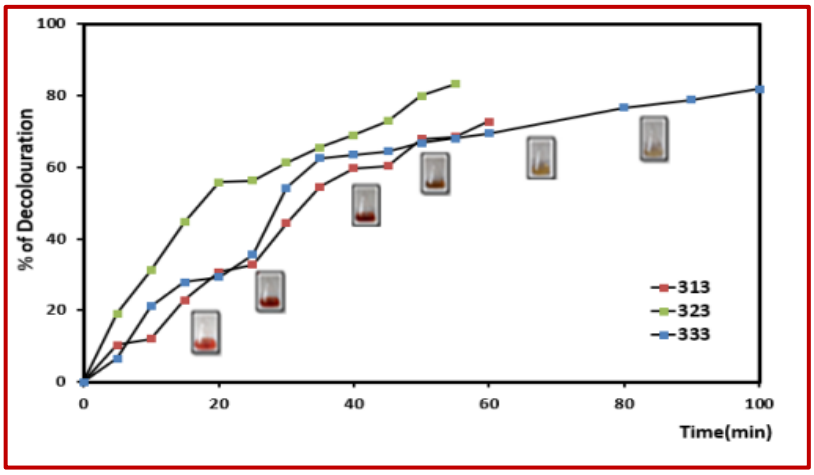

Fig. 11: Effect of time on MO decolorization using a Sm(III) catalyst at different temperatures

Table 11: Effect of time and temperature on M.O decolouration in presence of $[SmL_3](ClO_4)_3.H_2O$ catalyst

Temp (K) / Time (min)	**333**		**323**		**313**	
	% of decolouration	A°/A	% of decolo	A°/A	% of decolouration	**A°/A**
5	19.033	0.80	10.226	0.89	6.496	**0.93**
10	31.152	0.68	12.079	0.87	21.167	**0.78**
15	44.684	0.55	22.855	0.77	27.810	**0.72**
20	55.836	0.44	30.610	0.69	29.343	**0.70**
25	56.282	0.43	32.669	0.67	35.620	**0.64**
30	61.338	0.38	44.406	0.55	54.233	**0.45**
35	65.501	0.34	54.495	0.45	62.481	**0.37**
40	68.996	0.31	59.780	0.40	63.503	**0.36**
45	72.862	0.27	60.398	0.39	64.379	**0.35**
50	80.000	0.20	67.879	0.32	66.715	**0.33**
55	83.271	0.17	68.428	0.32	68.029	**0.32**
60	-	-	72.683	0.27	69.416	**0.31**
65	-	-	81.743	0.18	-	**-**
70	-	-	-	-	75.839	-
80	-	-	-	-	76.715	**0.23**
90	-	-	-	-	78.832	**0.21**
100	-	-	-	-	81.751	**0.18**

3.14.2. Kinetic study

The experimental data of methyl orange dye degradation acquired at three different temperatures, 313, 323, and 333 K were plotted as ln(A°/A) vs t, where A° and A referred to dye absorbance at the start and at time t, respectively (Figure 12). Good linear plots were produced for all the measured reaction temperatures, indicating that the breakdown of M.O dye proceeded a pseudo first-order response. Additionally, the easily determined slopes of the resulting graphs allowed the values of the reaction rate constants at each reaction temperature to be easily determined. The energy of activation E* was determined from the plot of log(k) vs 1/T (Figure 12). The energy of activation and other parameters are listed in Table 12. The negative activation values for entropy suggested that all of the compounds tested were highly ordered in their transition states. An examination of the kinetic variables revealed that the observed rate constant rises with increasing temperature (Arrhenius behaviour) [67]. As a result, this study provided valuable insight into the creation of new wastewater treatment pathways.

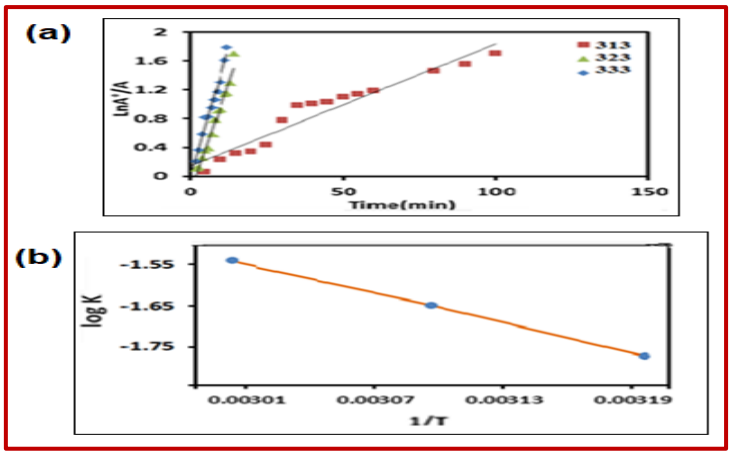

Fig. 12: (a) The relationship between ln A°/A and time, (b) the rate constants of M.O. decolorization at different temperatures in presence of a Sm(III) catalyst.

3.14.3. Mechanism

The first step is the adsorption of H_2O_2 at the surface of the catalyst, as well as metal reduction with the production of hydroperoxyl radicals ($HO_2^{\bullet}$). While $HO_2^{\bullet}$is a powerful oxidant, it is less efficient than $HO^{\bullet}$ generated in second step (2) by the addition of another molecule of H_2O_2. The radical species $HO^{\bullet}$ attack M.O molecules to give degradation products in the final step as follows:

$$\textbf{Catalyst} - M^{2+} + H_2O_2 \rightarrow \textbf{catalyst} - M^{1+} + HO_2^{\bullet} + H^+ \quad (1)$$

$$\textbf{Catalyst} - M^{1+} + H_2O_2 \rightarrow \textbf{catalyst} - M^{2+} + OH^- + HO^{\bullet} \quad (2)$$

$$\textbf{M.O} + HO^{\bullet} \rightarrow \textbf{Degradation products} \quad (3)$$

Table 12: Reaction rate and activation parameters of M.O decolouration

Complex formula	T (K)	K (min^{-1})	log(K)	ΔH^* (KJ/mol)	ΔS^* (J/mol)	ΔG^* (KJ/mol)	E^* (KJ/mol)
$[SmL_3](ClO_4)_3.H_2O$	31	0.017	-1.77	20.76	-	84.80	23.36
	32	0.023	-1.64	20.68	-	86.85	
	33	0.029	-1.53	20.59	-	88.90	

3.15. Pharmacological evaluation

3.15.1. In vitro antimicrobial activity

The antibacterial qualities of L and complexes were demonstrated in Figure 13. The moderate effectiveness of Ag(I) and U(VI) complexes against bacterial stains and C. albicans was evident. The greater efficiency for complexes over pure ligand based might be attributed to the permeation of cell notion [68,69] as well as Tweedy's chelation theory [70]. Metal ions, due to their high polarity, can scarcely move through the membrane enclosing the cell, according to the cell permeability idea. Furthermore, as π-electron delocalization rises across the entire ring of chelation, complex lipophilicity improves. As a result, the complexes' penetration across the membranes of lipids will be improved, and the sites of attachment of metal in microorganisms will be blocked [71].

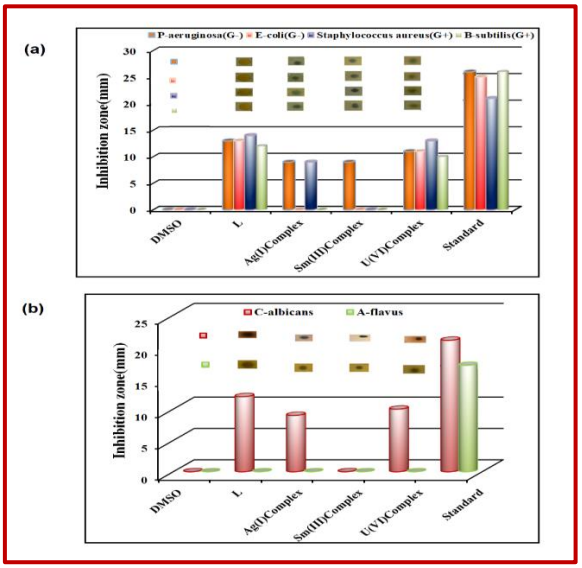

Fig. 13: Bioactivity of the ligand and its metal complexes against (a) bacteria and (b) fungi species

3.15.2. Cytotoxicity study

Many papers were evaluated demonstrating interest in using other metals get around and reducing the significant negative impacts of platinum compounds on patients [72,73].

Trials were performed in this study to investigated the ligand and its silver(I) complex as anticancer drugs. In *vitro* cytotoxicity caused by both the ligand and silver (I) complex on the breast cancer (MCF7) human cell line was evaluated and compared to the conventional cis-platin and doxorubicin. A substance is considered a strong antitumor agent if its IC50 activity is less than 5 g/mL. Moderate antitumor agents are substances with an IC50 activity between 5 and 10 g/mL, whereas weak anticancer drugs are those with an IC50 activity between 10 and 25 g/mL [74]. The researched chemicals exhibit varying anti-cell line actions. The IC_{50} values for the ligand L and Ag(I) complex against MCF7cell line are 81.5 ± 4.6 g/ml and 7.56± 0.3 g/ml, respectively [75,76]. The ligand L cannot be considered as an antitumor agent while the Ag(I) complex could be considered as a moderate antitumor drug. Figure 14 depicts the cytotoxicity results of the ligand and Ag(I) complex.

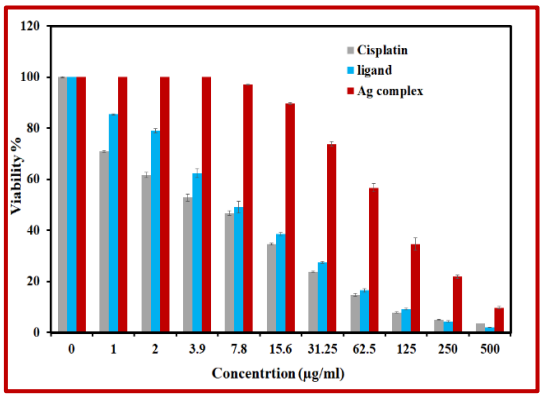

Fig. 14 : Cytotoxicity of ligand and Ag(I) complex against MCF-7 cell line

4. Conclusions

The nitrogen of the azomethine group and the oxygen atom of the furan ring serve as coordination sites for the ligand, L, which acts as a neutral bidentate-type. The Ag(I) complex has been proposed to have a tetrahedral structure, whilst the uranium (VI) and samarium (III) complexes possess six coordinated octahedral geometries. Thermal studies demonstrate that the complexes are extremely thermally stable. Except for U(VI), all the synthesized compounds have the potential to be photoactive. The pattern of X-ray diffraction of the ligand, Ag(I), and U(VI) complexes showed strong peaks, suggesting that they were crystalline, whereas the Sm(III) complex was amorphous. Gaussian 09 software was utilized to optimize the geometry of both ligand and silver(I) complex. From optimized structures, the DFT technique was utilized to compute bond length, angles of bonds, HOMO-LUMO energy gap, and quantum chemical parameters. The Sm(III) compound was discovered to catalyze dye degradation in the presence of H_2O_2, with a noticeable shift in the color of the product of the reaction with time and temperature. While the ligand may not be thought of as an antitumor drug, the Ag(I) complex may be considered a modest anticancer agent.

References

[1] E.A.M. Khalil, W.H. Mahmoud, M.M.I. El Dessouky, G.G. Mohamed, Egypt. J. Chem **64**, 3555 (2021). doi: 10.21608/ejchem.2021.71817.3578

[2] N.G. Zaki, W.H. Mahmoud, A.M. El Kerdawy, A.M. Abdallah, G.G. Mohamed, Spectrochim. Acta Part A: Mol. Biomol. Spectrosc. **229**, 117938 (2019). doi:10.1016/j.saa.2019.117938.

[3] E.A.M. Khalil, G.G. Mohamed, J. Mol. Struct. **1249**, 131612 (2022). doi:10.1016/j.molstruc.2021.131612.

[4] A. Pui, C. Policar, J.P. Mahy, Inorg. Chim. Acta **360,** 2139 (2007). doi:10.1016/j.ica.2006.10.040.

[5] A. Pui, Croatica Chem. Acta **75,** 165 (2002). https://hrcak.srce.hr/127493.

[6] L.S. Shul'pina, M.M. Vinogradov, Y.N. Kozlov, Y.V. Nelyubina, N.S. Ikonnikov, G.B. Shul'pin, Inorg. Chim. Acta **512,** 119889 (2020). doi:10.1016/j.ica.2020.119889.

[7] T. Măluţan , A. Pui, C. Măluţan, L. Tătaru, D. Humelnicu, J. Fluoresc. **18** (3-4), 707 (2008). doi:10.1007/s10895-008-0339-9.

[8] A. Bullock, M. Clemmons, Integrated Optics: Devices, Materials, and Technologies XXVI, 12004, 187 (2022). doi:10.1117/12.2605835.

[9] J. A. Cotruvo Jr, ACS central sci. **5**, 1496 (2019). doi:10.1021/acscentsci.9b00642

[10] G. N. Shao, Materials Research Foundations **132**, 97 (2022). doi:10.21741/9781644902110-5.

[11] Q. Zhang, S. O'Brien, J. Grimm, Nanotheranostics, **6**, 184 (2022). doi: 10.7150/ntno.65530.

[12] G. Bao, S. Wen., G. Lin, J. Yuan,K.-L. Wong, J.-C. G. Bünzli, D. Jin, Coord. Chem. Rev. **429**, 213642 (2022). doi: 10.1016/j.ccr.2020.213642.

[13] L. T. Wang, T. D. Solberg, P. M. Medin, R. Boone, Comp. in bio. and med. **31** (2), 101 (2001). doi:10.1016/s0010-4825(00)00026-3.

[14] C. Herlan, S. Bräse, Dalton Transactions **49**, 2397 (2020). doi:10.1039/C9DT04851K.

[15] S. Lahdenperä, Q. Wang, J. Vainio, T. Soukka, Analyst. **142,** 2411 (2017). DOI doi:10.1039/C7AN00199A.

[16] A. Pui, T. Malutan, L. Tataru, C. Malutan , D. Humelnicu , G. Carja, Polyhedron **30** (12), 2127 (2011). doi:10.1016/j.poly.2011.05.029.

[17] J. Gottfriedsen, F.T. Edelman, Coord. Chem. Rev. **251**, 142 (2007). doi:10.1016/j.ccr.2006.06.011.

[18] K. Wong, Y. Zhu, Y. Yang, G. Law, H. Fan, P.A. Tanner, W. Wong, Inorg. Chem. Commun. **12,** 52 (2009). doi:10.1016/j.inoche.2008.11.002.

[19] A. Alptürk, O. Rusin, W. Wang, J.O. Escobedo, I.M. Warner, W.E. Crowe, V. Kraál, J.M. Pruet, R.M. Strongin, PNAS **103** (26), 9756 (2006). doi:10.1073/pnas.0603758103.

[20] A. Zheng, J. Fan, B. Chen, X. Qin, J. Wang, F. Wang, R. Deng, X. Liu, Chem. Rev. 122 (6), 5519 (2022). doi:10.1021/acs.chemrev.1c00644.

[21] L. Lamiri, B. Kahouadji, M. Berd, A. Abdellatif, L. Benchallal, L. Guerbous, S. Ouhenia, A. Souici, L. Amiour, A. Zoukel, J. of Rare Earths **41** (1), 51 (2023). doi:10.1016/j.jre.2022.03.006.
[22] C. Marambio-Jones, E. M. Hoek, J. of nanopart. res. **12**, 1531 (2010).
[23] A.V Legler, A.S Kazachenko, O.V Kazbanov, Revyanova, Pharmaceutical J. **35** (9), 345 (2001).
[24] P. Ray, M. Cle´ment, C. Martini, I. Abdellah, P. Beaunier, J.´-L. Rodriguez-Lopez, V. Huc, H. Remita and I. Lampre, New J. Chem. **42**, 14128 (2018). doi:10.1039/c8nj02451k.
[25] A. Rosenani, A. W. Haque, and G. Tech Siang, Austrialian J. of Basic and Applied Sci., 5 (9), 365 (2011). ISSN 1991-8178.
[26] S.A. Emmanuel, S.A. Thomas, S.O. Idris, J.F. Iyun, AJCPR, 1, 38 (2013). www.pharmaresearchlibrary.com/ajcpr.
[27] M. Rendošová, R. Gyepes, M. Kello, M. Vilková, D. Mudroňová, P. Olejníková, P. Cardiano, S. Gama, D. Milea, Z. Vargová, J. Inorg. Biochem. **246**, 112266 (2023). doi: 10.1016/j.jinorgbio.2023.112266.
[28] M. Alizadeh, M. Jalal, A.S.K. Hamed, A. Saber, S. Kheirouri, F.P.F. Tabrizi, N. Kamari, J. Inflamm. Res. **13**, 451 (2020). doi:10.2147/JIR.S262132.
[29] A.A. Adeleke, Md. S. Islam, O. Sanni, C. Mocktar, S.J. Zamisa, B. Omond, J. Inorg. Biochem. **214**, 111266 (2021). doi:10.1016/j.jinorgbio.2020.111266.
[30] S.B. Aher, P.R. Inamdar, M. Kulkarni, M.V. Puri, S. Parekh, V. Bendre, Int. J. Life Sci. Pharma Res. **12**, L123 (2022). ISSN 2250-0480.
[31] Y. Sun, X. Huang, Y. Yue, W. Zhu, B. Zhang, R. Hou, A. Ishag, Ceramics International **49**, 40638 (2023). doi:10.1016/j.ceramint.2023.10.044.
[32] P. Li, J. Wanga, Y. Wanga, J. Lianga, D. Panc, S. Qiang, Q. Fan, J. of Photochem. and Photobio. C: Photochem. Rev. 41, 100320 (2019). doi:10.1016/j.jphotochemrev.2019.100320.
[33] H.E. Amin, O.A.M. Ali, S.M. EL-Medani, A.S. Sayed, J. of Sci. Res. in Sci. **36**, 1 (2019). doi:10.21608/JSRS.2019.30994.
[34] D. Staneva, E. Vasileva-Tonkova, I. Grabchev, Materials **12** (21), 3473 (2019). doi:10.3390/ma12213473.
[35] A. El-Sonbati, M. Diab, A. El-Bindary, A. Shoair, N. Beshry, J. of Mol. Liq. **218**, 400 (2016). doi:10.1016/j.molliq.2016.02.043.
[36] P. Wayne, Methods for dilution antimicrobial susceptibility test for bacteria that grow aerobically, Approved Standard-NCCLS document, 6th ed. (2003)
[37] S. N. Rampersad, Sensors **12** (9), 12347 (2012). doi:10.3390/s120912347.
[38] L.A. Al-Mutabagani, F.M. Abdelrazek, S.M. Gomha, A.S. Hebishy, M.S. Abdelfattah, S.M. Hassan, A.R. Sayed, M.M. Elaasser, App. Sci. **11** (19), 8908 (2021). doi:10.3390/app11198908.
[39] O.A.M. Ali, Z.H. Abd El–Wahab, B.A. Ismail, J. of Mol. Str. **1139**, 175 (2017). doi:10.1016/j.molstruc.2017.03.025.
[40] Z.H. Abd El–Wahab, O.A.M. Ali, B.A. Ismail, J. of Mol. Str. **1144**, 136 (2017). doi:10.1016/j.molstruc.2017.05.009.
[41] X.M. Zhang, J. Tang, L.N. Wang, D.Yao, Q. Yu, F.P. Huang, H.D. Bian, Polyhedron **133**, 433 (2017). doi: 10.1016/j.poly.2017.05.026.
[42] A.A.A. Aziz, F.M. Elantabli, H. Moustafa, S.M. El-Medani, J. of Mol. Str. **1141**, 563 (2017). doi:10.1016/j.molstruc.2017.03.081.
[43] B. Iftikhar, K. Javed, M. S. U. Khan, Z. Akhter, B. Mirza, V. Mckee, J. of Mol. Str. **1155**, 337 (2018). doi: 10.1016/j.molstruc.2017.11.022.
[44] O.A.M. Ali, S.M. El-Medani, M.R.A. Serea, A.S. Sayed, Spectrochimica Acta Part A: Mol. and Biomol. Spect. **136**, 651 (2015). doi:10.1016/j.saa.2014.09.079.
[45] M. Halli, R. Sumathi, Arabian J. of Chem. **10**, 1748 (2017). doi:10.1016/j.arabjc.2013.06.025.
[46] A.K. Sidhu, N. Verma, P. Kaushal, Frontiers in Nanotech **3**, 105 (2022). doi: 10.3389/fnano.2021.801620.
[47] M.S. El-Attar, H.S. Elshafie, S.A. Sadeek, A.F. El-Farargy, S.I. El-Desoky, W.H. El-Shwiniy, I. Camele, Chem. Biodiversity **19**, e202100785 (2022). doi:10.1002/cbdv.202100785.
[48] O.A.M. Ali, S.M. El-Medani, D.A. Ahmed, D.A. Nassar, J. of Mol. Str. **1074**, 713 (2014). doi:10.1016/j.molstruc.2014.05.035.
[49] T.E. Olalekan, A.S. Ogunlaja, B. VanBrecht, G.M. Watkins, J. of Mol. Str. **1122**, 72 (2016). doi:10.1016/j.molstruc.2016.05.098.
[50] S. Ramezani, M. Pordel, A. Davoodnia, Inorganica Chim. Acta **484**, 450 (2019). doi:10.1016/j.ica.2018.09.050.
[51] B. Shafaatian, Z. Ozbakzaei, B. Notash, S.A. Rezvani, Spectrochimica Acta Part A: Mol. and Biomol. Spect. **140**, 248 (2015). doi:10.1016/j.saa.2014.11.108.
[52] A.W. Coats, J. Redfern, Nature **201**, 68 (1964). doi: 10.1038/201068a0.
[53] T. Hatakeyama, F.X. Quinn, Thermal Analysis: Fundamentals and Applications to Polymer Science, 2 nd ed. (John Wiley, Chichester, 1999)
[54] H.I.M.M. EL-Shorbagy, El-Gendy, A.F. Belal, G. Hadad, Records of Pharmaceutical and Biomedical Sciences **7** (1), 27 (2023). doi:10.21608/RPBS.2023.166748.1177.
[55] G.G. Mohamed, M. M. Omar, A.M. Hindy, Turkish J. of Chem. **30**, 361 (2006). ISSN: 1300-0527.
[56] A. Frost, R. Pearson, Kinetics and Mechanism Inc., 2nd ed., (John Wiley and Sons, New York) **10,** (1961)
[57] B.A. Ismail, Z.H. Abd El-Wahab, O.A.M. Ali, D.A. Nassar, Scientific Rep. **13**, 9196 (2023). doi:10.1038/s41598-023-36060-0.
[58] D.A. Nassar, O.A.M. Ali, M.R. Shehata, A.S. Sayed, Heliyon **9**, e169732023 (2023). doi:10.1016/j.heliyon.2023.e16973.

[59] N. Ghosh, T. Chakraborty, S. Mallick, S. Mana, D. Singha, B. Ghosh, S. Roy, Spectrochimica Acta Part A: Mol. and Biomol. Spect. **151**, 807 (2015). doi:10.1016/j.saa.2015.07.050.
[60] N. Mohd Hapipi, J.K. Lim, S.K. Chen, O.J. Lee, A.H. Shaari, M.M. Awang Kechik, K.P. Lim, K.B. Tan, M. Murakami, M. Miryala, Crystals **9** (12), 655 (2019). doi:10.3390/cryst9120655.
[61] H.F. Abd El-Halim, G.G. Mohamed, E.A. Khalil, J. of Mol. Str. **1146**, 153 (2017). doi:10.1016/j.molstruc.2017.05.092.
[62] B.A. Ismail, D.A. Nassar, Z.H. Abd El–Wahab, O.A.M. Ali, J. of Mol. Str. **1227**, 129393 (2021). doi:10.1016/j.molstruc.2020.129393.
[63] S. Chakraborty, D.D. Purkayastha, G. Das, C.R. Bhattacharjee, P. Mondal, S.K. Prasad, D. S. Rao, Polyhedron **105**, 150 (2016). doi:10.1016/j.poly.2015.11.053.
[64] M.A. El-Ghamry, F.M. Elzawawi, A.A.A. Aziz, K.M. Nassir, S.M. Abu-El-Wafa, Scientific Rep. **12**, 17942 (2022). doi:10.1038/s41598-022-22713-z.
[65] V. Radha, S.J. Kirubavathy, S. Chitra, J. of Mol. Str. **1165**, 246 (2018). doi:10.1016/j.molstruc.2018.03.109.
[66] J. Wang, R. Bai, Water research **101**, 103 (2016). doi:10.1016/j.watres.2016.04.044.
[67] A.S. Elsherbiny, H.A. El-Ghamry, Intern. J.of Chem. Kinetics **47**, 162 (2015). doi:10.1002/kin.20900.
[68] D.J. Benos, D.W. Deamer, A. Kleinzeller, D.M. Fambrough, Membrane permeability: 100 years since Ernest Overton, Academic Press, (San Diego London Boston, New York, Sydney Tokyo Toronto), (1999).
[69] E. M. Komyha, W. H. Mahmoud, W. M. Hosny, A. A. El-Sherif, Egypt. J. Chem. **66**, 1219 (2023). DOI: 10.21608/EJCHEM.2023.147796.6650
[70] B. Tweedy, Phytopathology **55**, 910 (1964).
[71] V.P. Singh, A. Katiyar, S. Singh, Biometals **21** (4), 491 (2008). doi:10.1007/s10534-008-9136-9.
[72] A. M. F. Galal, K. Mahmoud, Egypt. J. Chem. **64**, 3465 (2021). DOI: 10.21608/EJCHEM.2021.64272.3381
[73] V. Brabec, O. Nováková, Drug Resistance Updates **9**, 111 (2006). doi:10.1016/j.drup.2006.05.002.
[74] N. Cutillas, G.S. Yellol, C. de Haro, C. Vicente, V. Rodríguez, J. Ruiz, Coord. Chem. Rev. **257**, 2784 (2013).doi:10.1016/j.ccr.2013.03.024
[75] M. A. Franco-Molina, E. Mendoza-Gamboa, C. A. Sierra-Rivera, R. A. Gómez-Flores, P. Zapata-Benavides, P. Castillo-Tello, J. M. Alcocer-González, D. F. Miranda-Hernández, R.S. Tamez-Guerra, C. Rodríguez-Padilla, J. of Exper. & Clinical ancer Res. **29**, 148 (2010). doi: 10.1186/1756-9966-29-148.
[76] S. Jarre, I.Raya, P. Prihantono, R. Arfah, M Gappa, St. Fauziah, S. Santi, R. Irfandi, Egypt. J. Chem. **66**, (2023). DOI:10.21608/EJCHEM.2022.149508.6466
[77]